BECKMAN COULTER
Life Sciences

Demystifying DGE-AUC Part 2: Physical Principles and Links to Preparative DGUC

Akash Bhattacharya
Beckman Coulter Life Sciences, 4510 Byrd Dr, Loveland, CO 80538

Abstract:

This application note is the second in a technical series which will cover the basics of density gradient equilibrium analytical ultracentrifugation or DGE-AUC. In this installment, we discuss DGE-AUC in detail covering its physical basis, drawing parallels to preparative density gradient ultracentrifugation or DGUC. We also discuss the DGE-AUC workflow and look at data on density gradients formed by different chemicals. Finally, we discuss the optimization of density gradients with experimental examples.

Introduction:

Background

In the first part of this series, Demystifying DGE-AUC Part 1: Back to the Basics, we introduced the science of Analytical Ultracentrifugation (AUC)[1], along with historical perspective on its development[2]. We also provided a comparison of several AUC experimental techniques and their use cases. We then introduced a resurging orthogonal technique known as density gradient equilibrium analytical ultracentrifugation, or DGE-AUC. We compared DGE-AUC to the preparative technique of density gradient ultracentrifugation or DGUC, which is used to purify viruses, extracellular vesicles and other biologics[3,4]. Finally, we showed the results of simulating DGE-AUC data and discussed its utility.

In this application note, we will continue our exploration of DGE-AUC in more detail. This includes the detection and visual representation of DGE-AUC data and optimization of experiments. DGE-AUC is based on the same physical principles governing preparative DGUC. A DGE-AUC experiment necessitates the simultaneous monitoring of the behavior of the gradient forming material (GFM), as well as the analyte. This is demonstrated with examples. The selection of GFMs is discussed with considerations like chemical and optical compatibility with the sample. Finally, an overall workflow for DGE-AUC is presented, along with experimental data on the optimization of density gradients.

Upcoming installments in this series will delve into setting up DGE-AUC experiments, analyzing DGE-AUC data, optimizing experiments to enhance analyte signal, and featuring case studies involving biologic samples like AAVs and LNPs.

DGE- AUC

The physical principles behind DGE-AUC

The physical principle behind DGE-AUC is as follows: analyte particles are mixed with a GFM and centrifuged at high speed. At equilibrium the GFM forms a density gradient from the top to the bottom of the AUC sample cell following the same quadratic exponential curve shape that is obtained in a sedimentation equilibrium experiment[5].

$$c(r)=c_0 \cdot \exp\left(\frac{M_b \cdot \omega^2}{RT} \cdot \left(\frac{r^2-r_0^2}{2}\right)\right)$$

In this equation, the concentration c(r) is a function of radius r. The reference concentration c_0 is defined at reference radius r_0, and M_b is the buoyant mass of the analyte. The angular velocity is ω. R is the Universal Gas Constant and T is the temperature.

This is the first of two transport processes which are occurring simultaneously in the AUC cell.

1. The first transport process relates to the gradient forming material (GFM) while the second transport process relates to the movement of the actual analyte particle, which may be a protein, a nucleic acid, a virus, a nanoparticle, etc.

2. The second transport process relates to the analyte particles. This process also attains its own equilibrium wherein different analyte particles in solution migrate to a radial position where the local density of the gradient forming material is equal to the buoyant density of the analyte particle in question. Thus, at equilibrium a DGE-AUC experiment separates analytes on the basis of their buoyant densities.

DGE-AUC and DGUC

The physical principle behind DGE-AUC is the same as in density gradient ultracentrifugation or DGUC. Thus, it is worthwhile to discuss the mechanics of DGUC and contrast it with sedimentation ultracentrifugation.

In preparative ultracentrifugation, a mixture of analyte and impurity can be separated by simple sedimentation experiments, provided that the analyte and impurities differ with respect to sedimentation coefficient, allowing one material to form a pellet while the other remains in solution. This form of purification requires solutions without GFMs and can be utilized in successive or cascading "pelleting" steps, with intermediate processes such as resuspension and washing of the pelleted material in the previous step. Each step yields a slightly higher purity target.

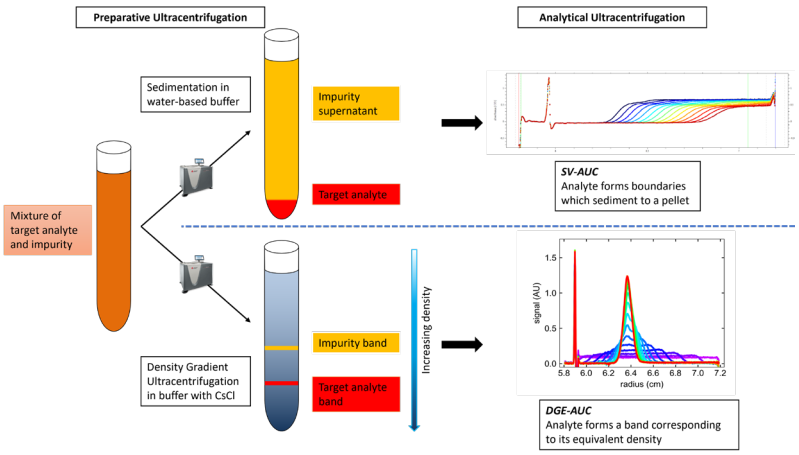

Figure 1. Schematic showing sedimentation ultracentrifugation vs density gradient ultracentrifugation

Density gradient ultracentrifugation (DGUC) on the other hand, involves ultracentrifugation of a mixture of analyte and impurity in a buffer containing a GFM such as cesium chloride or CsCl. At equilibrium, CsCl forms a density gradient from low density at the top of the tube (inner radius) to high density at the bottom of the tube (outer radius). The analyte and impurity will both accumulate as bands at the radial position where the local density corresponds to their respective buoyant density. In the schematic shown here in Figure 1, the impurity is shown to accumulate at a higher band (lower density) as compared to the analyte. The analytical equivalent is shown on the right side, wherein sedimentation in the sample with water-based buffer leads to the formation of bands which move toward the cell bottom accumulating as a pellet, while in the sample with CsCl, the analyte accumulates as a band which increases in height and decreases in width over time until equilibrium is reached.

In a mixture of AAV capsids, containing fully loaded and empty capsids we would expect the fully loaded capsids (which are of higher density) to stabilize at a radial position further down the sample tube as compared to empty capsids (which are lower density). A similar effect is seen for drug-carrying nanoparticles where the empty nanoparticle has a different density from the drug-loaded nanoparticle. Figure 2 shows the result of DGUC performed on a mixture of circular high-density plasmid and linearized (enzymatically cleaved) low-density plasmid in CsCl. The high-density plasmid appears further down the sample tube as compared to the low-density "nicked" plasmid.

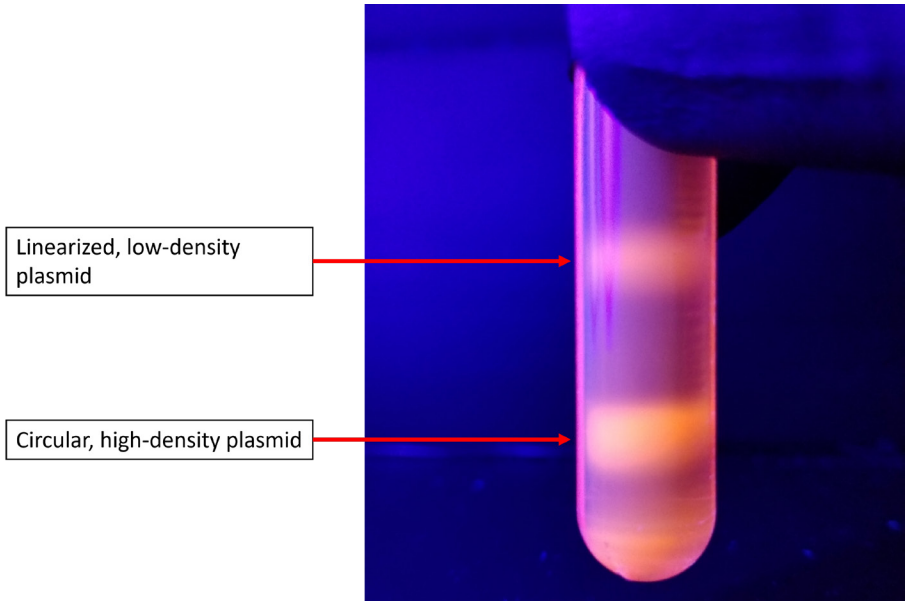

Figure 2. DGUC of a mixture of circular (high-density) and linearized (low-density) plasmid

DGE-AUC workflow

Detection of AUC data

The modern AUC instrument, the Optima AUC, has two optical systems which can be used simultaneously: a UV-vis absorbance (Abs) detector and a Rayleigh Interference Fringe (RIF) detector[6]. The absorbance detector system records light intensity as a function of radius for both sectors (Ireference and Isample). The light source used is a Xenon flash lamp with a wavelength range from 190 to 800 nm. Detection is via a photomultiplier tube (PMT) followed by operational amplifier stages. The Optima AUC software converts the intensity readings into absorbance readings using the formula:

$$\text{Abs} = -\log \frac{I_{\text{reference}}}{I_{\text{sample}}}$$

These absorbance values are available for the radial range of 5.8 to 7.2 cm at intervals of 10 μm – leading to ~ 1400 datapoints per scan, which can be downloaded and plotted.

The Rayleigh interference detector operates on a different principle. This detector illuminates both sectors of the AUC cell with a 660 nm laser. The optical path difference between light passing through the two sectors, resulting from concentration differences, leads to the formation of fringes which are then captured by a CCD camera with a resolution of 2048 x 1088 pixels. These fringes are then Fourier transformed to yield plots of Rayleigh Interference Fringe shifts (RIF) vs radius (with a radial resolution of 2K), which can then be downloaded and plotted.

Anatomy of an AUC scan

For both detector systems, the scans are timestamped. Thus, a single AUC scan consists of some form of signal as a function of radius, at a given time. This is shown in Figure 3.

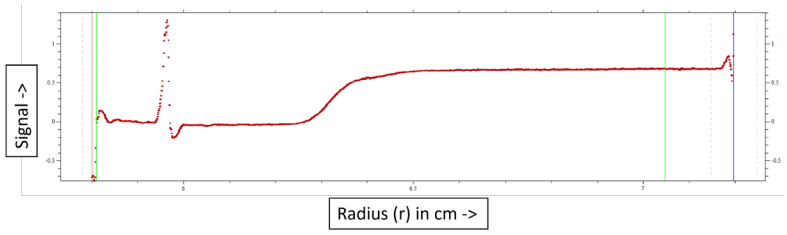

Figure 3. Anatomy of an AUC scan

Simultaneous monitoring of both GFM and analyte

Typically, the GFM is monitored via the interference system while the analyte of interest is monitored via the absorbance system. Thus, it is possible to monitor the GFM and the analyte independently and thus ensure that both transport processes have attained equilibrium before analyzing the data and interpreting the results. This is seen in Figure 4, where panel A shows the approach to equilibrium of CsCl, as monitored by RIF scans, where panel B shows the approach to equilibrium of AAV, as monitored by absorbance at 230 nm.

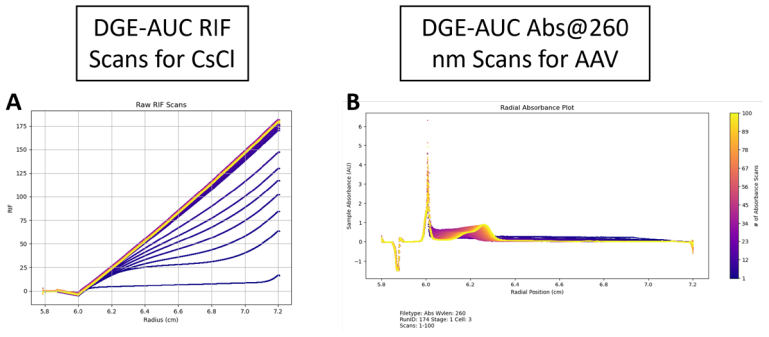

Figure 4. Simultaneous monitoring of GFM (CsCl) and analyte (AAV)

Simple DGE-AUC workflow

A schematic of the overall DGE-AUC workflow is shown in Figure 5. This workflow assumes that we start with an optimized GFM. An initial experiment is performed with the GFM and the analyte to determine if any absorbance mode signal is attributable to the analyte or not. In the case we do not observe the absorbance signal, it may be required to perform some biochemical troubleshooting. Typical considerations include whether the sample or analyte has been degraded in the presence of the GFM or buffer, any unexpected chemical interactions resulting in loss of absorbance signal, etc. It may be required at this stage to reject the GFM altogether and search for a better alternative. Assuming that absorbance signal is detected and can be attributed correctly to the analyte of interest, the next question is whether the analyte sediments or floats under the applied experimental conditions. Either condition means that this experiment is effectively an SV-AUC experiment and not a DGE-AUC experiment. It may be necessary to adjust the GFM concentration and reduce rotor speed. If these steps lead to observable DGE peaks, then we proceed to optimize the position and height of the peaks by altering GFM starting density, rotor speed and temperature as well as sample concentration. Once the experiment is optimized, the data can be analyzed and interpreted.

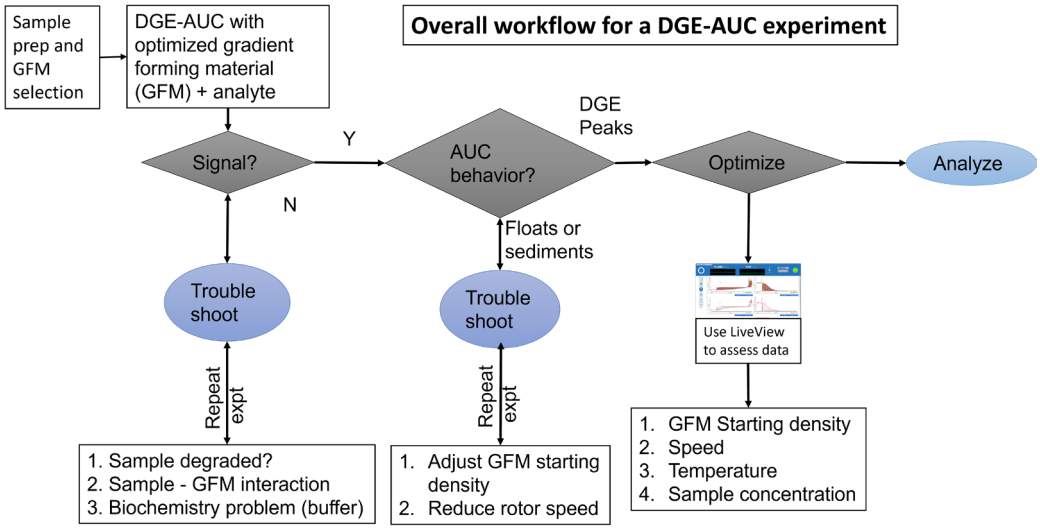

Figure 5. Workflow for a DGE-AUC experiment

Selection of Gradient Forming Material (GFM):

The DGE-AUC workflow shown in Fig 5 assumes that we have a sample/analyte in solution with a suitable gradient forming material (GFM). Finding a suitable GFM is by no means a trivial task and may require some optimization as shown below in Figure 6.

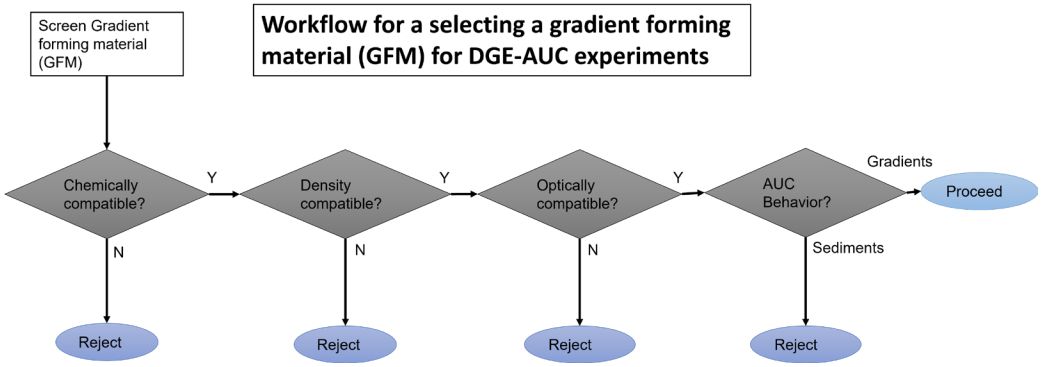

Figure 6. Workflow to select GFM

Chemical Compatibility

Figure 6 shows the workflow for selecting the appropriate gradient forming material or GFM. The first step is to decide whether the gradient forming material is chemically appropriate or not. This step is important because choosing an inappropriate gradient forming material may alter the actual analyte we are interested in studying. For instance, while a salt like cesium chloride is a suitable gradient forming material for virus particles, its high ionic strength makes it chemically incompatible with lipid nanoparticles (LNPs) and liposomes.

Density Selection

The second consideration is one of suitable density. For example, CsCl has a saturation density of approximately 1.9 g/mL. Therefore, it is well suited to act as a GFM for virus particles such as adeno associated virus or AAV, which typically display a density of 1.35g/mL. However, for an analyte like LNP the expected density range might be between 1.0 and 1.1 g/mL. In this case, it might be better to use a lower-density GFM such as sucrose.

Optical Compatibility

The third consideration is that of optical compatibility. A GFM may be chemically suitable for the analyte in question as well as provide the correct density range, but if its absorption is too high at the wavelength of interest then it will not be useful. For instance, Optiprep™ or Iodixanol is chemically suitable for a wide range of biological samples as well as possesses an appropriate density range. However, it has an exceptionally high absorption at 230 nm. This precludes Iodixanol as a GFM in DGE-AUC for virus particles, LNPs and various other analytes which are usually detected at 230 nm. In our study, we have used sucrose as the GFM for analyzing liposomes and LNPs. This is because of the density range accessible by sucrose solutions, chemical compatibility (sucrose is frequently used as a cryoprotectant for liposomes[7]) as well as the low absorption at the wavelengths of interest (especially at 230 nm). Furthermore, sucrose has a high refractive index, allowing it to be easily monitored by the interference detector in the Optima AUC. The optical behavior of sucrose is shown in Fig 7.

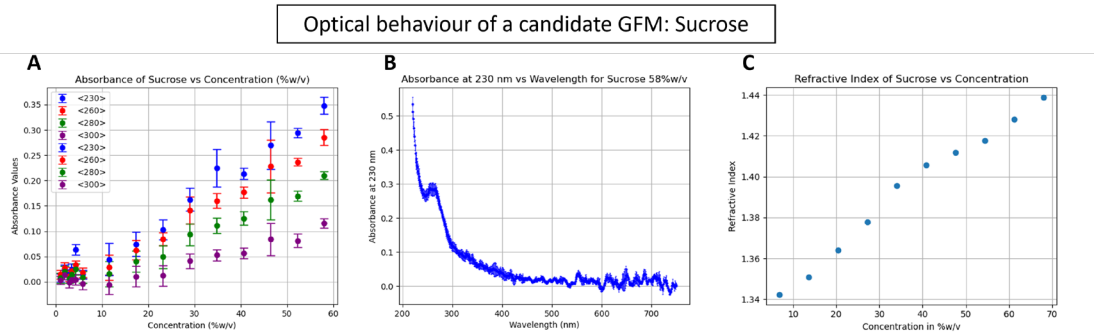

Figure 7. Optical behavior of sucrose; 7A: Absorbance (10 mm path) of sucrose at different wavelengths vs concentration; 7B: Full spectrum of sucrose at 58% w/v, and 7C: Refractive Index of sucrose vs concentration

Centrifugation Behavior

The last consideration is that of the behavior of the GFM under centrifugation. If the GFM itself is made of very large-sized particles, then it will sediment even at low rotor speeds. Examples can be seen with GFMs that are composed of silica nanoparticles such as Percoll® and Percoll® Plus. Both of these GFMs sediment very easily even at 10,000 RPM rotor speed and are therefore unsuitable for most biological analytes.

Common Gradient Forming Materials

GFMs commonly used in preparative ultracentrifugation are good candidates for DGE-AUC – but many of these chemicals will fail the compatibility screens. Examples of a few commonly used gradient forming materials are shown in Table 1. Additional resources can be found here[8].

Gradient Forming Material (GFM)	Class / Family	Max Density (g/ml)	Chemical Compatibility	Optical compatibility at 230/260/280 nm	On Centrifugation
Cesium Chloride	heavy salt	1.9	viruses	Yes	Gradients
Percoll®	colloidal silica nanoparticles	1.135	cells	Yes	Sediments
Percoll® Plus	colloidal silica nanoparticles	1.3	cells	Yes	Sediments
Ficoll®	Polysaccharide	1.077	cells	No	Gradients
Ficoll-Paque®	Polysaccharide + iodine salt	1.077	cells	No	Gradients
Sucrose	Disaccharide	1.55	cells, viruses, LNP, liposomes	Yes	Gradients

Table 1. Several common gradient forming materials

Experimental data on GFMs:

The density gradient is monitored via the interference detector system. This detector converts RIF images into scan data with fringe shift on the Y axis and radial position on the X axis via Fourier transforms. The transform algorithm sometimes introduces radially independent shifts in the baseline as well. In addition, raw RIF scans also fail to show the pivoting of density gradients around the isodensity position. Thus, it is worthwhile to explore the features of a RIF scan as shown in Figure 7.

Morphology of experimental DGE-AUC RIF data for a GFM

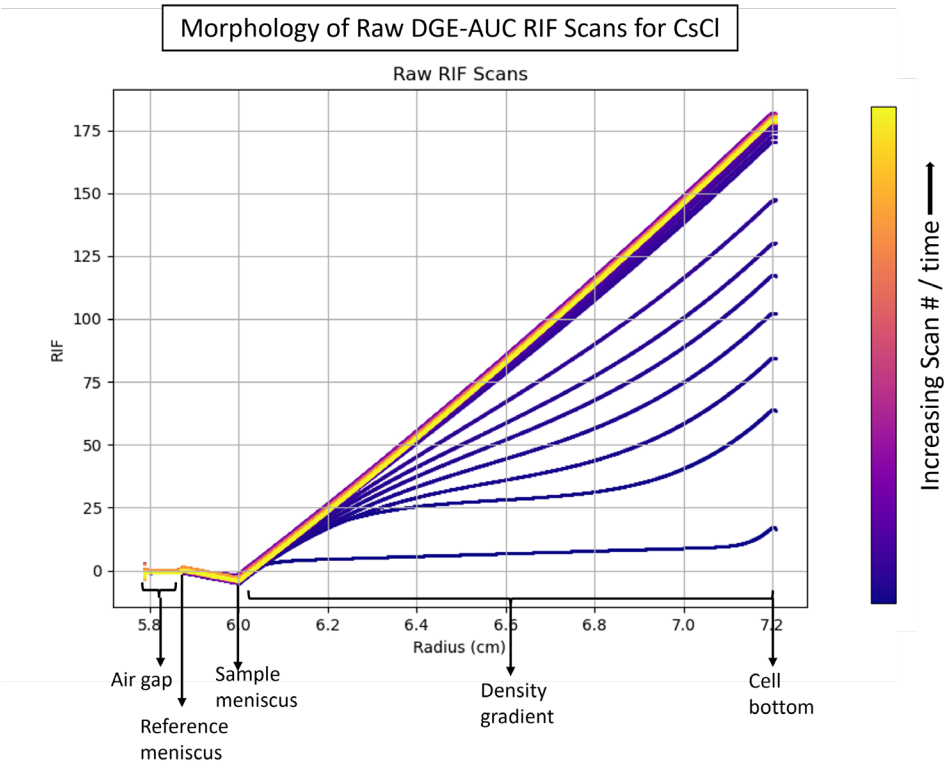

Figure 8. Features of a RIF scan: DGE-AUC of KBr at 1.1 g/ml in PBS run at 40 krpm, 20C

In Figure 8, the region from 5.8 to 5.84 cm corresponds to the air gap. The reference meniscus is seen at 5.84 cm. The region from 5.84 to 6.0 cm corresponds to reference loaded / sample empty, with the sample meniscus seen at 6.0 cm. Thereafter, the actual density gradient is seen from the sample meniscus at 6.0 cm to the cell bottom at 7.2 cm.

The isodensity point

As mentioned previously, at equilibrium, a GFM forms a curve wherein its concentration can be written as a function of radius described by a quadratic exponential curve. It can be shown that a radial position exists where the GFM concentration is the same as the starting or loading concentration. This radial position is called the isodensity or pivot point. The simulations of density gradient curves shown in Part 1 of this series show that the curves are formed by the concentration profile pivoting around the isodensity point as GFM is depleted from the inner radii and accumulates at the outer radii. This is seen in Figure 9.

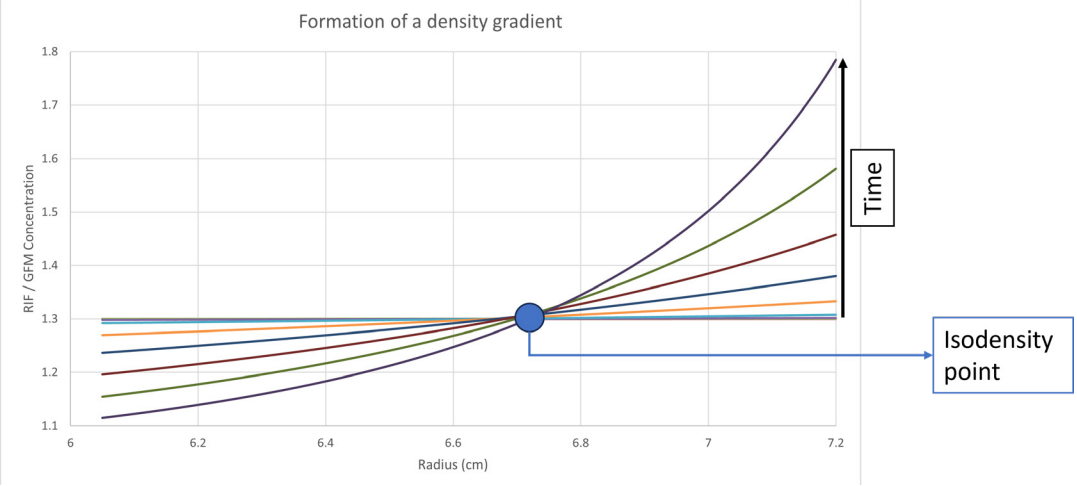

Figure 9. Density gradient curves pivoting around the isodensity point

The isodensity point corresponds to the approximate radial position given by the equation[9]

$$r_{iso} = \frac{r_b^2 + r_m^2}{2}$$

Where r_b corresponds to cell bottom and rm corresponds to the meniscus radius.

Transformation of RIF scan data

The RIF system is sensitive, but not selective. RIF scan data shows the behavior of not just the GFM, but any component of the overall sample loaded into the AUC cell which has a refractive index different from that of PBS buffer (or other reference buffer). This includes species like CsCl, which are expected to form a gradient, but also biologics like proteins, nucleic acids, etc. – which are expected to sediment. Thus, two data transform operations are performed:

Baselining with respect to the air gap:

In order to gauge the differences between successive RIF scans in any AUC experiment, it is desirable to baseline all the scans using the air gap. This operation is particularly useful when the RIF scan data will be used for analyzing SV-AUC data and is shown in Figure 10, panel B. This also allows us to better visualize when some components are sedimenting instead of forming a gradient, which can be very useful while screening for GFMs. In addition, if the analyte itself has a high refractive index and has a significant contribution to RIF signals, baselining with respect to the air gap can be useful in identifying such analytes.

Baselining with respect to the isodensity point:

Assuming that the two problems mentioned above have been solved (i.e., the analyte does not contribute measurably to RIF signal and the GFM is not sedimenting, but only forming a gradient), a different form of baselining is needed. Thus, when the RIF system is being used to monitor GFMs only, and the scan data will not be used for SV-AUC analysis, then it is necessary to render the scans similar to the simulations shown previously. Thus, we show in Figure 10, panel C – the results of baselining the RIF scans with respect to the isodensity point. Upon doing so, the scans are seen to pivot around this point as the experiment progresses. The pivot angle changes with time until equilibrium is established. This allows us to best gauge when equilibrium has been established.

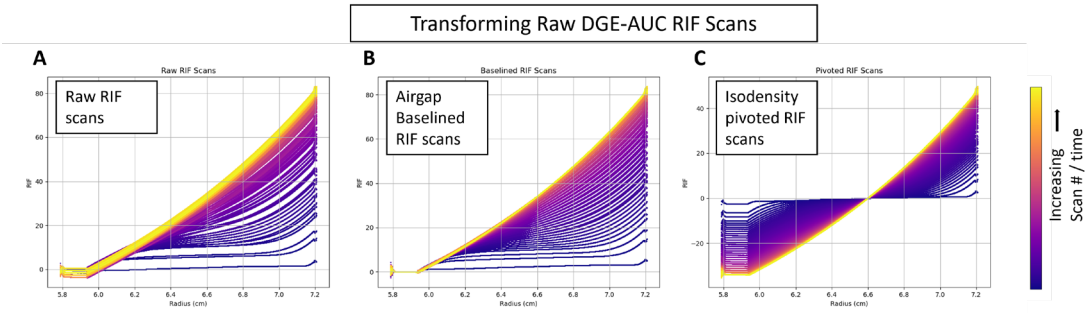

Figure 10. Adjustment of RIF scans for DGE-AUC of 3.5% w/v sucrose in PBS run at 40krpm, 20°C. A: Raw data, B: Baselined using the air gap, C: Baselined using the isodensity point

Examples of equilibrium density gradients formed by different GFMs.

The speed with which equilibrium is attained, as well as the shape of the final DGE curve, is dependent on the nature of the GFM. Examples are shown below in Figure 11 for four GFM candidates. Panel A shows KBr at a density of 1.1 g/mL in PBS, panel B shows CsCl at 1.35 g/mL in PBS, panel C shows sucrose at 3.5 % w/v in PBS and panel D shows Dextran at 4% w/v in PBS. The experiment was carried out at 40 krpm and 20 °C. The RIF scans for KBr, CsCl and Sucrose were baselined around the isodensity point. This transformation was not carried out for Dextran due to its markedly different behavior. The following observations can be made:

Species	KBr	CsCl	Sucrose	Dextran
Approximate time to equilibrium	10 hrs	8 hrs	1 day	N/A
Dynamic RIF Range	80 fringes	180 fringes	70 fringes	300 fringes

Table 2. DGE behavior for different candidate GFMs

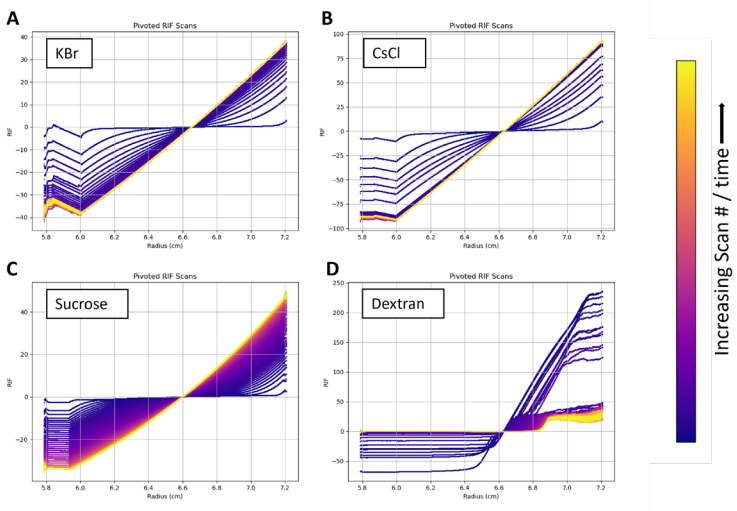

Figure 11. Approach to density gradient equilibrium for different GFMs

In addition, we note that:

1. Dextran shows a very interesting pattern of mixed sedimentation and equilibrium formation. This suggests that it is not suitable for use as a GFM, even though it may be chemically compatible with many biological analytes.
2. It can be seen for three of the GFMs (KBr, CsCl and sucrose) that the RIF scan pattern switches from horizontal at the outset of the experiment, to a shallow S-shaped curve as the experiment progresses to finally settle on the concave-upward shape at equilibrium. Sucrose displays a more curved shape for the final density gradient as compared to KBr and CsCl. Thus, observation of the RIF curve shape is a useful diagnostic for whether the GFM has attained equilibrium. A S-shape indicates that transport dynamics are still in play and equilibrium has not been attained.

Optimization of DGE curves

Referring to Figure 5, the optimization of a DGE-AUC experiment involves the adjustment of: (i) GFM starting (loading) concentration or density, (ii) rotor speed, (iii) experiment temperature and (iv) sample or analyte starting (loading) concentration. The first three parameters can and should be tested without the presence of analytes to better understand the DGE behavior of the GFM. This is illustrated below. In all cases, the GFM RIF scans are baselined with respect to the isodensity point.

Variation of DGE curve shape with rotor speed

At equilibrium, the shape of the density gradient should correspond to the theoretical concave-upward shape as shown in the simulations previously. The gradient curves become progressively steeper as rotor speed is increased. This is shown for three common GFMs below in Figure 12. These GFMs are the same as shown previously in Fig 11 (with the omission of dextran): KBr at a density of 1.1 g/mL in PBS (Fig 12A), CsCl at 1.35 g/mL in PBS (Fig 12B) and sucrose at 3.5 % w/v in PBS (Fig 12C). Rotor speeds of 5, 10, 20, 30 and 40 krpm were tested, all at 20°C. The different equilibrium curves all pivot around the isodensity point. Again, the equilibrium curve for sucrose exhibits slightly greater curvature as compared to KBr and CsCl.

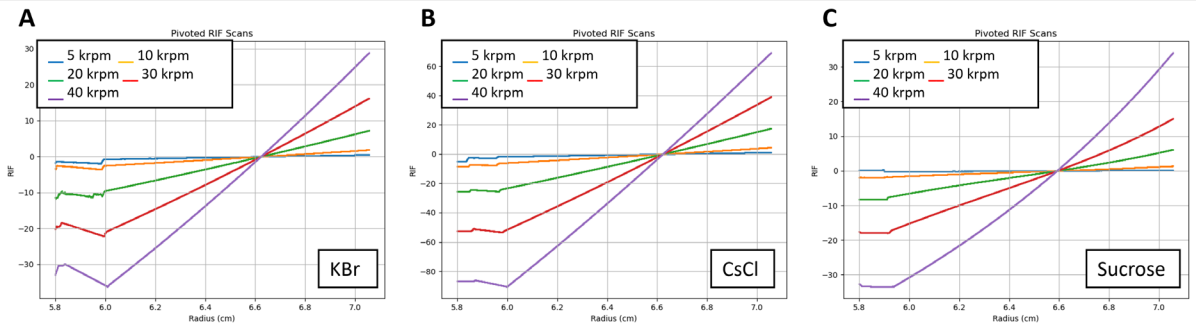

Figure 12. Variation of DGE curve profiles with rotor speeds for different GFMs

Variation of DGE curve shape with temperature

Diffusion of the GFM decreases with temperature. Therefore, at lower temperatures, we expect to see that DGE curves become slightly steeper. This effect is shown in Figure 13 for the same three GFMs shown previously. Fig 13A: KBr, Fig 13B: CsCl and Fig 13C: sucrose. The experiments were carried out at a rotor speed of 40 krpm and at temperatures of 20 °C (blue trace), 10 °C (orange trace) and 4 °C (green trace). The steepening effect with decreased temperature is seen for all three GFMs.

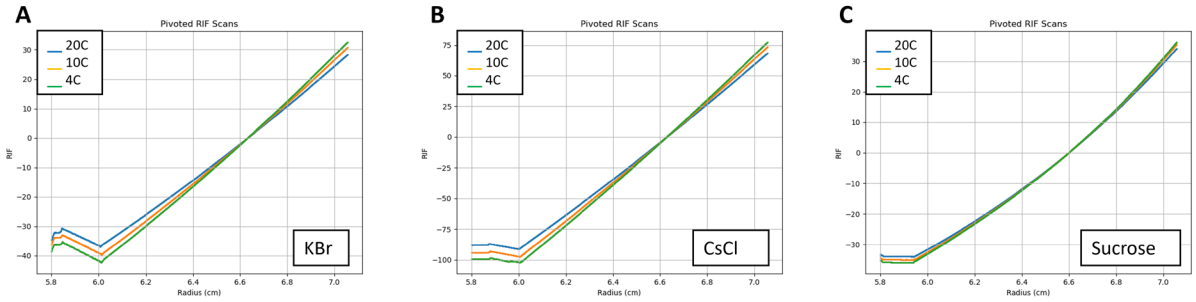

Figure 13. Effect of temperature on density gradient shape.

Variation of DGE curve shape with GFM starting concentration

The effect of GFM initial concentration/density on DGE shape can also be predicted via simulations. In Figure 12, we show the DGE curves resulting from three samples of CsCl in PBS at densities of 1.35 g/mL (blue trace), 1.33 g/mL (orange trace) and 1.37 g/mL (green trace) at temperatures of 20°C (panel A) and 4°C (panel B). The rotor speed in all cases was 40 krpm. It is observed that the higher concentration shows a slightly greater dynamic range. It must be noted, however, that these density gradient curves are not at equilibrium – as seen by their S-shape. The curves correspond to a timepoint of roughly 4 hrs after commencement of the experiment (following a 4 hr temperature equilibration stage).

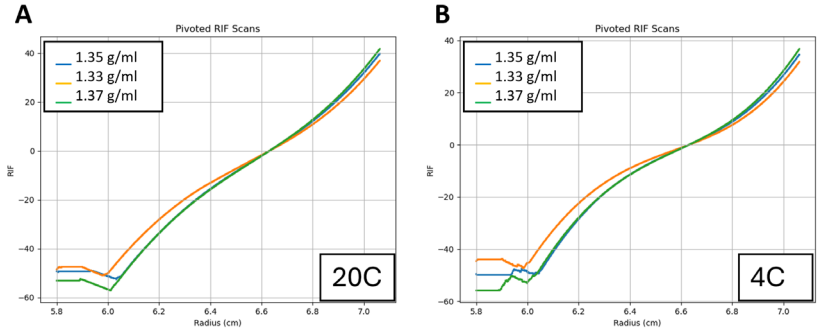

Figure 14. Effect of temperature on DGE curves for CsCl. A: 20°C, B: 4°C

Summary and Conclusions

In this installment of the Demystifying DGE series of application notes, we have covered the following topics: the physical principles behind DGE-AUC, its relationship to preparative DGUC, the DGE-AUC workflow, including AUC signal detection and data acquisition modes, the anatomy of an AUC scan and the use of absorbance and interference detectors to simultaneously monitor both the analyte as well as the GFM. We explored the selection criteria for GFMs in more detail, considering chemical, optical and centrifugation behavior, and evaluated AUC scans corresponding to some common GFM candidates. Finally, we have explored the optimization of DGE experiments by adjustment of GFM starting concentrations, rotor speed and experiment temperature with experimental data for candidate GFMs like CsCl and Sucrose.

Disclaimer

1. Several third-party software vendors supply programs for the analyses of the raw data generated by the Beckman Coulter Inc. ("Beckman") Analytical Ultracentrifuge. Third-party analysis software has not been validated by Beckman for use with the Beckman Analytical Ultracentrifuge. Training conducted by Beckman on the third-party software, does not imply a recommendation for use or the suitability of the third-party software use by the customer. Beckman does not endorse any third-party analyses software. Beckman warranty and/or performance guarantee that may be applicable or are provided by Beckman for Beckman Analytical Ultracentrifuge do not apply to any third-party software.

2. Copyright, License and Terms of Use Disclaimers are documented for the below software on their respective pages. For example:

    a. SEDDFIT: **https://sedfitsedphat.nibib.nih.gov/software/default.aspx**

    b. OriginLab: **https://www.originlab.com/index.aspx?go=Company/TermsOfUse**

    c. Ultrascan: **http://ultrascan.aucsolutions.com/license.php**

    d. Microsoft: **https://www.microsoft.com/en-us/useterms/**

    e. Gussi: **https://www.utsouthwestern.edu/labs/mbr/software/**

    f. Python: **https://www.python.org/**

    g. Matplotlib: **https://matplotlib.org/**

    h. NumPy: **https://numpy.org/**

    i. SciPy: **https://scipy.org/**

    j. MATLAB: **https://www.mathworks.com/products/matlab.html**

3. Beckman Coulter makes no warranties of any kind whatsoever express or implied, with respect to this protocol, including but not limited to warranties of fitness for a particular purpose or merchantability or that the protocol is non-infringing. All warranties are expressly disclaimed. Your use of the method is solely at your own risk, without recourse to Beckman Coulter. Not intended or validated for use in the diagnosis of disease or other conditions. This protocol is for demonstration only and is not validated by Beckman Coulter.

4. Regulatory / Trademark Statements:

    a. All products and services identified, unless noted as for in-vitro diagnostic (IVD) use, are for research use and not intended or validated for use in the diagnosis of disease or other conditions.

    b. ©2024 Beckman Coulter, Inc. Beckman Coulter, the stylized logo, and the Beckman Coulter product and service marks mentioned herein are trademarks or registered trademarks of

    c. Beckman Coulter, Inc. in the United States and other countries.

References:

1. Cole, J. L. & Hansen, J. C. Analytical ultracentrifugation as a contemporary biomolecular research tool. J Biomol Tech 10, 163-176 (1999).

2. Nobel Prize Physics 1926 Summary, **<https://www.nobelprize.org/prizes/physics/1926/summary/> (1926)**.

3. Lane, R. E., Korbie, D., Trau, M. & Hill, M. M. Purification Protocols for Extracellular Vesicles. Methods Mol Biol 1660, 111-130 (2017). **https://doi.org/10.1007/978-1-4939-7253-1_10**

4. Nasukawa, T. et al. Virus purification by CsCl density gradient using general centrifugation. Arch Virol 162, 3523-3528 (2017). **https://doi.org/10.1007/s00705-017-3513-z**

5. Cole, J. L., Lary, J. W., P Moody, T. & Laue, T. M. Analytical ultracentrifugation: sedimentation velocity and sedimentation equilibrium. Methods Cell Biol 84, 143-179 (2008). **https://doi.org/10.1016/S0091-679X(07)84006-4**

6. Beckman Analytical Ultracentrifuges, **<https://www.beckman.com/centrifuges/analytical-ultracentrifuges/optima-auc> (2023)**.

7. Boafo, G. F. et al. The Role of Cryoprotective Agents in Liposome Stabilization and Preservation. Int J Mol Sci 23 (2022). **https://doi.org/10.3390/ijms232012487**

8. Hinton, R. & Dobrota, M. Laboratory Techniques in Biochemistry and Molecular Biology. (North Holland Publ.Comp., 1976).

9. Savelyev, A., Brookes, E. H., Henrickson, A. & Demeler, B. A new UltraScan module for the characterization and quantification of analytical buoyant density equilibrium experiments to determine AAV capsid loading. Eur Biophys J 52, 311-320 (2023). **https://doi.org/10.1007/s00249-023-01641-4**

For Beckman Coulter's worldwide office locations and phone numbers, please visit Contact Us at **beckman.com**
2024-GBL-EN-105902-v1

BECKMAN COULTER
Life Sciences

danaher